Climate Dynamics (1999) 15:369–387

W. May

Space-time spectra of the atmospheric intraseasonal variability in the extratropics and their dependency on the El Niño/Southern Oscillation phenomenon: model versus observation

Received: 25 August 1997 / Accepted: 2 December 1998

Abstract By comparing the results obtained from two sets of simulations with the ECHAM3 and the ECHAM4 atmospheric general circulation models with results derived from the ECMWF re-analyses, we not only investigate the models' capability to reproduce aspects of the intraseasonal variability in the extratropics realistically, but also evaluate the impact of the changes between the two different versions of the ECHAM model. Moreover, we assess the impact of the marked variations of sea surface temperatures in the tropical Pacific associated with the El Niño/Southern Oscillation (ENSO) phenomenon on the characteristics of the intraseasonal variability in the midlatitudes. Both models realistically reproduce many aspects of the intraseasonal variability in the extratropics, i.e. the partition of the variability into the contributions of the transient cell and of the stationary and transient eddies and its seasonal variation, and also the spectral distribution of the contribution of the transient waves to the intraseasonal variability. The most severe deficiency of the models is a considerable underestimation of the contributions of the transient waves to the intraseasonal variability, mainly in the low-frequency part of the spectrum. In the recent version of the ECHAM model (ECHAM4) some of the model's shortcomings in simulating the intraseasonal variability realistically, in particular those in the Southern Hemisphere, are noticeably reduced compared to the previous version (ECHAM3). Yet some aspects are more realistically captured by ECHAM3. Both the ECMWF re-analyses and the two sets of simulations with the ECHAM models reveal a distinct impact of the ENSO phenomenon on the characteristics of the intraseasonal variability within the extratropics in boreal winter. In the Northern Hemisphere the most prominent effect is that the activity of the stationary waves is enhanced during El Niño events at the expense of the transient waves. In the Southern Hemisphere, on the other hand, all the different contributions to the variance on intraseasonal time scales (transient cell, transient and stationary eddies) are stronger during El Niño than during La Niña events. Concerning the transient waves, this mainly reflects changes in the low-frequency part of the spectrum associated with the activity of ultra-long planetary waves.

W. May
Danish Meteorological Institute, Lyngbyvej 100,
DK-2100 Copenhagen, Denmark
E-mail: may@dmi.dk

1 Introduction

Various phenomena on different spatial and temporal scales contribute to the intraseasonal variability in the extratropics (e.g. Blackmon 1976). Baroclinic disturbances such as travelling cyclones with a typical lifetime of a few days affect the day-to-day variability of the atmosphere. Large-scale flow anomalies such as blocking anticyclones or cut-off lows (e.g. Rex 1950a, b; Blackmon et al. 1986) may last for several weeks. These transient fluctuations on different scales, however, influence each other via non-linear interactions, in particular their temporal evolution and spatial distribution (e.g. Mullen 1987).

A method for distinguishing the contributions of the transient fluctuations on different spatial and temporal scales to the intraseasonal variability is the wave number-frequency analysis (e.g. Hayashi 1982). This technique also provides a partition of the variance due to transient fluctuations in an eastwardly and a westwardly propagating component, a standing component and the noise introduced by errors in the observations (Deland 1972).

During the last two decades there have been numerous studies of wave number-frequency spectra computed from observational data (e.g. Pratt and Wallace 1976; Fraedrich and Böttger 1978; Mechoso

and Hartmann 1982; Speth and Madden 1983) and also some studies based on model data (e.g. Pratt 1979; Hayashi and Golder 1977, 1983), but no one had used data from a present-day state-of-the-art general circulation model (GCM) for investigating the intraseasonal variability in the extratropics. More recently Hayashi and Golder (1993) studied intraseasonal oscillations in the tropics by means of a wave number-frequency analysis based on data originating from a state-of the-art model. Over the last decade GCMs have become more and more important and have demonstrated their capability to simulate the present-day climate represented by seasonal mean values quite realistically. Therefore it is of relevance to investigate whether these models also reproduce the variability on intraseasonal time scales realistically, in particular the dependency of the variability on spatial as well as temporal scales.

GCMs have also shown their capability to reproduce the observed and well-established impact of the El Niño/Southern Oscillation (ENSO) phenomenon on the seasonal mean circulation in the extratropics realistically (e.g. Hoerling et al. 1992; May and Bengtsson 1998), but so far nothing is known about the GCMs' capability to simulate the impact of the ENSO phenomenon on the intraseasonal variability in the midlatitudes. Though the effect of the ENSO phenomenon on the intraseasonal variability in the extratropics is not well-established, there is some observational evidence of a change in the spectral distribution of the intraseasonal variability in the Northern Hemisphere midlatitudes during El Niño (warm ENSO-events) as well as during La Niña events (cold ENSO-events) (Hansen et al. 1989; Fraedrich and Müller 1993). May and Bengtsson (1996) found a change in both the strength and the location of the main stormtracks and in the occurrence of persistent large-scale flow anomalies such as blocking anticyclones and cut-off lows in the Northern Hemisphere extratropics depending on the phase of ENSO.

In the present study we compare the results obtained from two sets of simulations with the ECHAM3 and ECHAM4 atmospheric GCM with results derived from the ECMWF re-analyses in order not only to investigate the models' capability to reproduce aspects of the intraseasonal variability in the extratropics realistically, but also to evaluate the impact of the changes between the two different versions of the ECHAM model. Changes in the recent version of the model (ECHAM4) relative to ECHAM3 are substantial both in the numerical methods and the physical parametrizations (Roeckner et al. 1996). Our study includes both the Northern and the Southern Hemisphere, since the different topographic forcing of the stationary waves induces some interhemispheric differences. Moreover, we assess the impact of the marked variations of sea surface temperatures (SSTs) in the tropical Pacific associated with the ENSO phenomenon on the characteristics of the intraseasonal variability in the midlatitudes, given the simulations with the ECHAM model as well as the re-analyses.

The work is organized as follows: in Sect. 2 we describe the data used in this study, and in Sect. 3 the results obtained from the re-analyses. In sect. 4 we compare the results derived from the two sets of simulations with the ECHAM3 and the ECHAM4 atmospheric GCMs with those based on the re-analyses. Subsequently we investigate the impact of the ENSO phenomenon as indicated in the re-analyses (Sect. 5) as well as in the two sets of simulations (Sect. 6). A summary and some concluding remarks follow in section 7.

2 Data

The models employed are the ECHAM3 and the ECHAM4 atmospheric GCMs at a horizontal resolution of T42 and 19 vertical levels (DKRZ 1992). Both models were developed at the Max-Planck-Institute for Meteorology for simulating the present day global climate and a possible global change in climate due to enhanced emissions of greenhouse gases. They are based on the global forecasting system that is used at the European Centre for Medium-Range Weather Forecasts (ECMWF). However, several major changes have been made, in particular to the physical parametrizations in order to make the model suitable for climate simulations. For a detailed description of ECHAM3 we refer to Roeckner et al. (1992) or Bengtsson et al. (1996). Details on ECHAM4 can be found in Roeckner et al. (1996).

Relative to the ECHAM3 model, ECHAM4 has undergone substantial changes in both the numerical methods and the physical parametrizations (Roeckner et al. 1996). Moisture and cloud water are advected using a semi-Lagrangian advection scheme (Williamson and Rasch 1994). The radiation scheme is based on the two-stream approach of the radiative transfer function with six spectral bands in the terrestrial (Morcrette 1991) and two in the solar part of the spectrum (Fouquart and Bonnel 1980). It includes additional greenhouse gases such as methane, nitrous oxide, numerous CFCs and various types of aerosols. The water vapour continuum has been revised according to Giorgetta and Wild (1995). The scattering properties of cloud droplets and ice crystals are parametrized as in Rockel et al. (1991). A high-order closure scheme is applied to compute the turbulent exchange of momentum, heat, moisture and cloud water within and above the atmospheric boundary layer (Brinkop and Roeckner 1995). The eddy diffusion coefficients are calculated as functions of the turbulent kinetic energy, which is obtained from the specific rate equation. As in ECHAM3 the convective mass flux scheme according to Tiedtke (1989) is used. The closure for deep convec-

tion and organized entrainment, however, has been modified and is now based on buoyancy instead of the moisture budget (Nordeng 1994). The organized detrainment is calculated for a spectrum of clouds detraining at different heights. Moreover, a data set of land-surface parameters corresponding to Claussen et al. (1994) is used, and the parametrization of the horizontal diffusion has been modified (Roeckner et al. 1996). In ECHAM4 a high-order closure scheme, which confines the damping to the high-wave number end of the spectrum, has been introduced.

A comparison with the operational ECMWF analyses (Roeckner et al. 1996) reveals that some of the biases in ECHAM3 remain virtually unchanged in ECHAM4. The polar upper troposphere and lower stratosphere, for instance, are much too cold, inducing very large errors in the zonal wind component above the 200 hPa level. The errors in the temperature and zonal wind component within the troposphere are generally smaller than in the previous version, except for the tropics, where the overestimation of Walker-type circulations in the equatorial plane is even more pronounced and the simulation of the Indian summer monsoon is less realistic. The most substantial improvements compared to ECHAM3 are found in the land surface climate. The temperature and precipitation errors, for instance, are generally smaller than before. These improvements can be attributed to an improved presentation of surface radiation fluxes via larger absorption of solar radiation in the atmosphere due to both water vapour and clouds.

We have performed five individual simulations with ECHAM3 over a period of approximately 14 y each and two individual simulations with ECHAM4 over a somewhat longer period of approx. 15 y. In each simulation a sequence of observed monthly mean values of the SSTs and of the sea-ice extent for a global ocean have been given as lower boundary forcing, but different atmospheric initial conditions have been prescribed. These data have been derived from observed monthly mean values of the SSTs and the sea-ice extent for the period September 1979 to December 1992 for the simulations with ECHAM3 and to December 1993 for the simulations with ECHAM4. For the period 1979 to 1988 we have used the AMIP-dataset (Gates 1992) and for the subsequent years data from NMC/CAC (Reynolds 1988). The five simulations with ECHAM3 have already been used in May (1994), May and Bengtsson (1996, 1998) and Bengtsson et al. (1996), the two simulations with ECHAM4 in Roeckner et al. (1996).

As observational data we use the ECMWF re-analyses for the period September 1979 through December 1993 (Gibson et al. 1997). For the purposes of our study we have reduced the data to T42, the same horizontal resolution as the simulations. Both the model and the observational data have been available two times daily at 00 and 12 UTC.

3 ECMWF re-analyses

3.1 Analysis of variance

The total variance of the geopotential height field associated with longitudinal and temporal variations can be separated into three different parts: the contributions of the transient cell and of the stationary and transient eddies. Details on the procedure we have applied in order to obtain these contributions are given in Appendix A.

Figure 1 shows the longitudinal and temporal means of these contributions to the variance of the geopotential height at 500 hPa for the ECMWF re-analyses as well as for the two sets of simulations with the ECHAM model (see Sect. 4.1). The values correspond to the long-term means computed from the re-analyses and the ensemble means obtained from the sets of five simulations with ECHAM3 and of two simulations with ECHAM4 for the extratropical regions of both hemispheres that are the zones between 40° and 70° northern and southern latitude, respectively. In order to compute the area averages over these zones the estimates at a given latitude have been weighted with the cosine of the latitude.

According to the re-analyses, the different contributions to the variance undergo marked variations in the course of the year in both hemispheres. The contributions of the stationary and the transient eddies are strongest in local winter and weakest in summer, and the values in local spring exceed those in autumn. The contributions of the transient cell, on the other hand, are considerably enhanced during the transition seasons with the values in local autumn

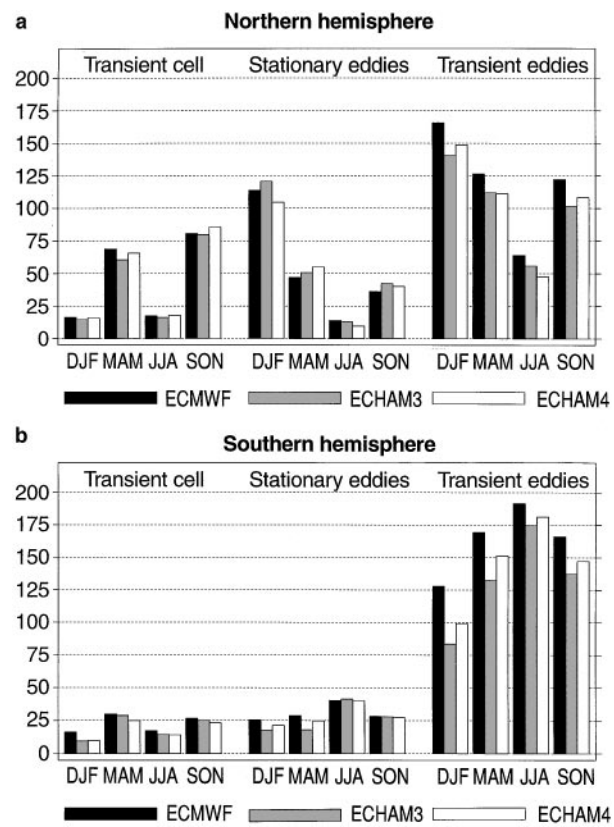

Fig. 1a, b Contributions of the transient cell and the stationary and transient eddies to the variance of the geopotential height at 500 hpa distinguishing between different data sets and different seasons. The values represent area averages over the zone between 40° and 70° **a** northern and **b** southern latitude, respectively. Units are 100 m^2

exceeding those in spring. The seasonal variations are much stronger in the Northern than in the Southern Hemisphere, in particular for the transient cell and the stationary eddies.

3.2 Wave number-frequency analysis

In order to characterize the contributions of the transient eddies to the atmospheric intraseasonal variability by their longitudinal and temporal scales we perform a wave number-frequency analysis of the contributions of the transient eddies to the variance of the geopotential height at 500 hPa. The method applied is described in further detail in Appendix B.

3.2.1 Northern Hemisphere

In the following we show variance spectra derived from the ECMWF re-analyses as well as from the two sets of simulations with the ECHAM model (see Sect. 4.2). The estimates represent the long-term means computed from the re-analyses and the ensemble means derived from the sets of five simulations with ECHAM3 and of two simulations with ECHAM4. In order to compute the area averages over the zone between 40° and 70° northern and southern latitude, respectively, the spectral estimates at a given latitude have been weighted with the cosine of the latitude. The comprehensive presentation for each data set is double-logarithmic with the period on the abscissa and the zonal wave number ranging from 1 to 10 on the ordinate. The spectral densities were multiplied by the wave number and frequency in order to emphasize spectral peaks.

The left column of Fig. 2 shows the variance spectra in the northern midlatitudes obtained from the ECMWF re-analyses in boreal winter. The total spectrum gives a fair amount of variability for all the wave numbers and periods shown, indicating three prominent planetary wave regimes. On time scales longer than 10 days, which we will refer to as the low-frequency part of the spectrum, the ultra-long planetary waves at wave numbers 1, 2 and 3 give major contributions to the intraseasonal variability. On time scales shorter than 6 days, the high-frequency part of the spectrum, the variability is mainly caused by the baroclinic waves at wave numbers 6 and higher. On intermediate time scales between 6 and 10 days the long planetary waves at wave numbers 4 and 5 give major contributions to the intraseasonal variability. While the variance on intermediate and short time scales is mainly due to propagating disturbances, in the low-frequency part of the spectrum the propagating and standing waves contribute to the same extent to the total variance. The variance spectra derived from the ECMWF re-analyses for the Northern Hemisphere are in good agreement with those of Fraedrich and Böttger (1978) and Hansen et al. (1989), whose spectra were based on different data.

3.2.2 Southern Hemisphere

The right column of Fig. 2 shows the variance spectra in the southern midlatitudes obtained from the re-analyses in austral winter. The total spectrum gives a fair amount of variability for all the wave numbers and periods shown, but in contrast to the Northern Hemisphere only two prominent planetary wave regimes appear. On time scales shorter than 6 days the variability is mainly caused by the planetary waves at wave numbers 5, 6 and higher, whereas on time scales between 6 and 16 days the long planetary waves at wave numbers 3 and 4 give major contributions to the intraseasonal variability. The variance on these scales is more than twice that in the Northern Hemisphere in boreal winter. The ultra-long waves at wave numbers 1 and 2 contribute about one third less to the intraseasonal variability than in the Northern Hemisphere. It is mainly the propagating disturbances that are responsible for these interhemispheric differences. The propagating variance spectrum also exhibits the pronounced peaks on intermediate time scales at wave number 4 and on shorter temporal scales at wave number 5. The standing variance spectrum reveals enhanced variability at wave number 3, whereas the ultra-long waves at wave number 1 and 2 do not contribute as much to the standing variance as in the Northern Hemisphere. The variance spectra obtained from the ECMWF re-analyses for the Southern Hemisphere are in good agreement with the results of Fraedrich and Kietzig (1983) and Hansen et al. (1989) and power spectra of the sea-level pressure by Mechoso and Hartmann (1982). The differences between the Northern and the Southern Hemisphere can be attributed to the different topographic forcing in the two hemispheres, as was pointed out by Hayashi and Golder (1983).

4 Echam model

In this section we investigate to which extent ECHAM3 and ECHAM4 are capable of reproducing the variability on intraseasonal time scales in the extratropics realistically. Moreover, we study the impact of the substantial changes, which the ECHAM model has undergone (see Sect. 2), on the simulation of the intraseasonal variability.

4.1 Analysis of variance

Both the ECHAM3 and the ECHAM4 model show the partition of the variability into the contributions of the transient cell and of the transient and stationary eddies in agreement with the re-analyses. In addition, they reveal the same seasonal variations and interhemispheric differences of these contributions to the variance as in the re-analyses (Fig. 1). However, the contributions as simulated by the two models are characterized by some marked differences relative to the re-analyses and some pronounced differences between the two versions of the ECHAM model. According to a two-sided t-test (e.g. Essenwanger 1986) the differences discussed in the following are significant at a level of 95% or even 99%.

The most severe deficiency of the models is the underestimation of the contributions of the transient disturbances. In the Southern Hemisphere this shortcoming of the ECHAM model is considerably reduced in ECHAM4, while in the northern midlatitudes this is only the case in boreal autumn and winter. Here the disagreement is worse in the recent version of the model in boreal summer. With regard to the stationary eddies, the quality of the simulation in the southern midlatitudes is also improved in ECHAM4, in particular in austral summer and autumn, whereas in the Northern Hemisphere the simulations with ECHAM3 are more realistic. In the northern midlatitudes the contribution of the transient cell is greater in the recent version of the model than in the previous one, leading to a better agreement with the re-analyses in all seasons but boreal

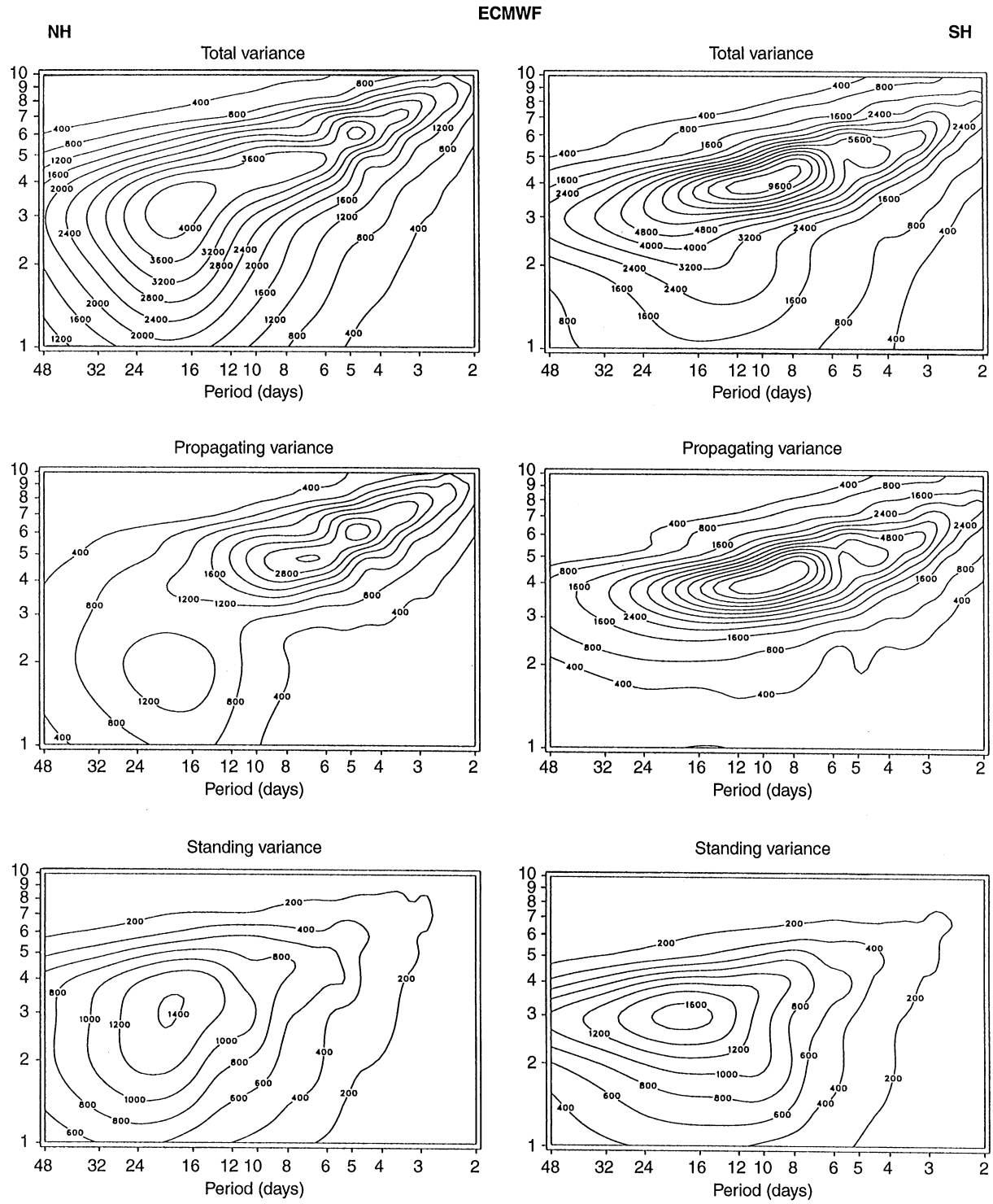

Fig. 2 Variance spectra of the geopotential height at 500 hPa in boreal winter between 40°–70 °N (*left*) and in austral winter between 40°–70 °S (*right*) obtained from the ECMWF re-analyses. The spectral estimates are multiplied by wave number and frequency. For the Northern Hemisphere the contour interval is 400 m^2 for the total and propagating variance, 200 m^2 for the standing variance, and for the Southern Hemisphere the contour interval is 800 m^2 for the total and propagating variance (the 400 m^2 contour line is indicated as well), 200 m^2 for the standing variance. The *zonal wave number* is given on the *ordinate*

autumn, when the contribution of the transient cell is too strong. In the Southern Hemisphere, on the other hand, this transient cell is weaker in ECHAM4 than in ECHAM3 resulting in a more severe underestimation of its contribution to the variance in the recent version of the ECHAM model.

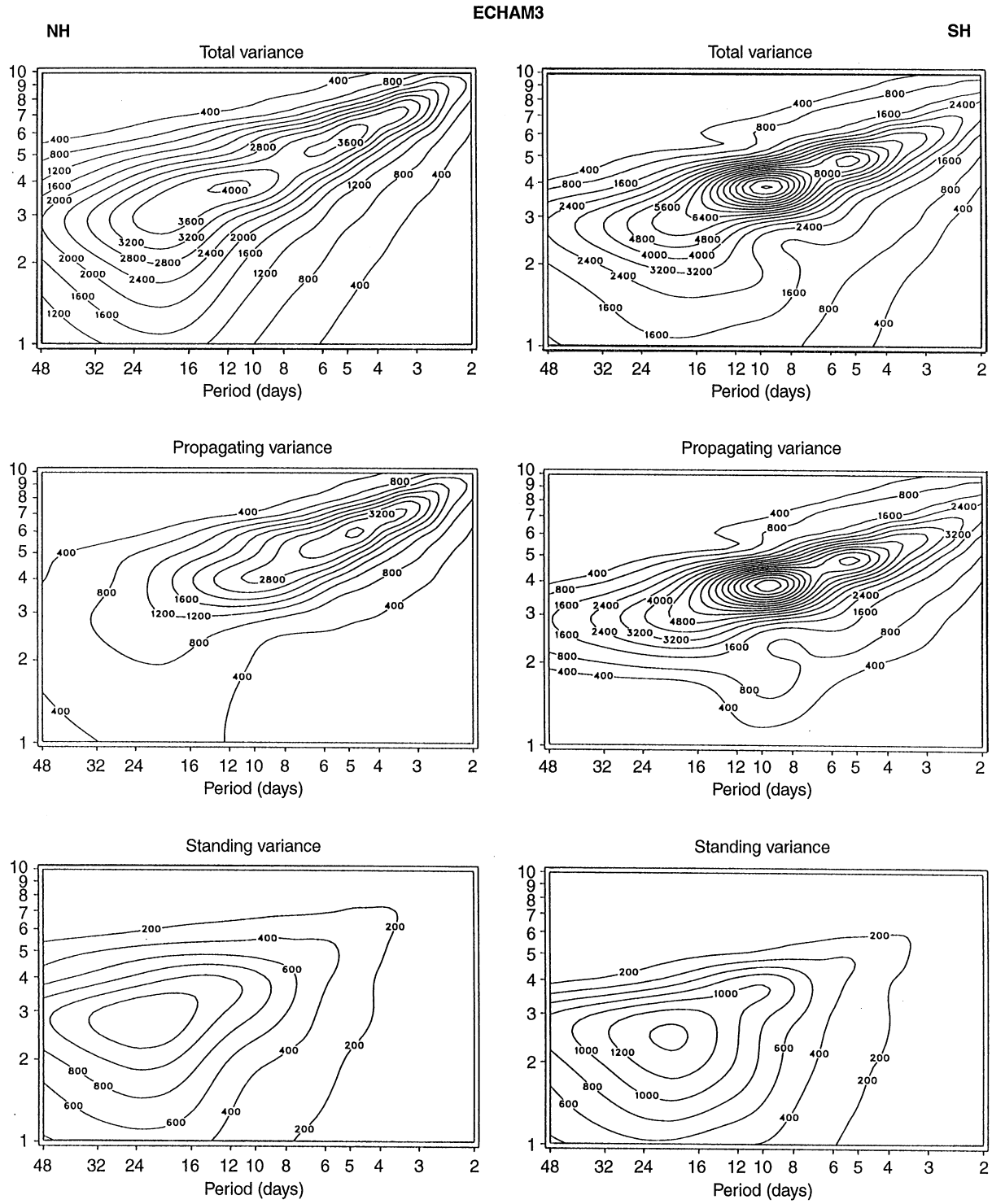

Fig. 3 As Fig. 2, but for the simulations with ECHAM3

4.2 Wave number-frequency spectra

4.2.1 Northern Hemisphere

The variance spectra in the northern midlatitudes obtained from the two sets of simulations with the ECHAM model in boreal winter (Figs. 3 and 4) have the same general structure as in the ECMWF reanalyses (Fig. 2), that is the partition of the variance onto short and long spatial and temporal scales. But several essential differences can be noted. In the total variance spectrum obtained from the simulations with

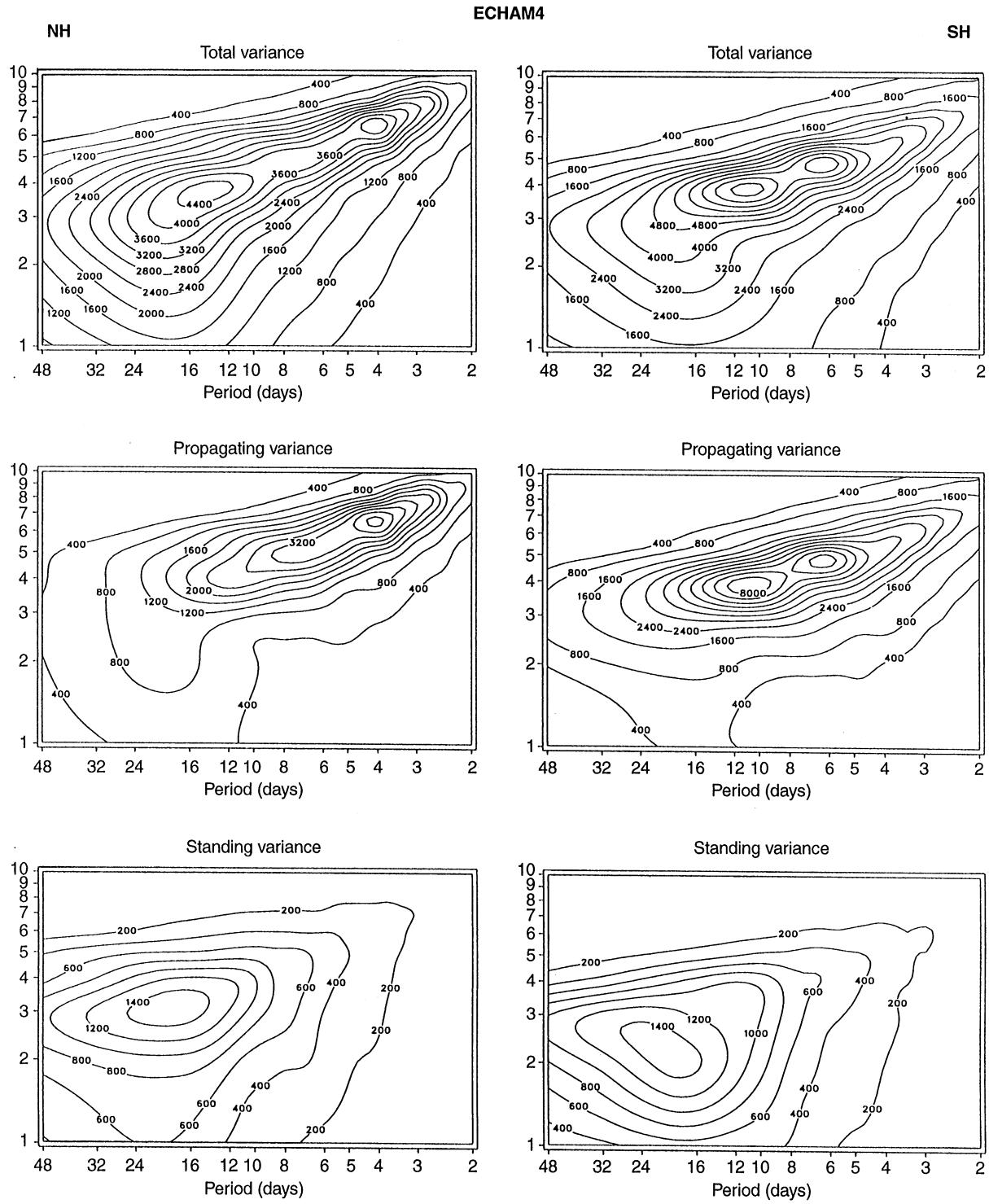

Fig. 4 As Fig. 2, but for the simulations with ECHAM4

ECHAM3 (Fig. 3), for instance, the three characteristic regimes are not as pronounced as in the re-analyses. This is not just an artifact due to the averaging over the five individual simulations, as none of the spectra calculated from the individual simulations show these regimes clearly (May 1994). The propagating variance spectrum does not reveal these three peaks either, in particular not the one in the low-frequency part of the spectrum. Here, where the ultra-long waves contribute greatly to the intraseasonal variability, the standing variance exceeds the propagating variance in contrast to the re-analyses. In the simulations with ECHAM4

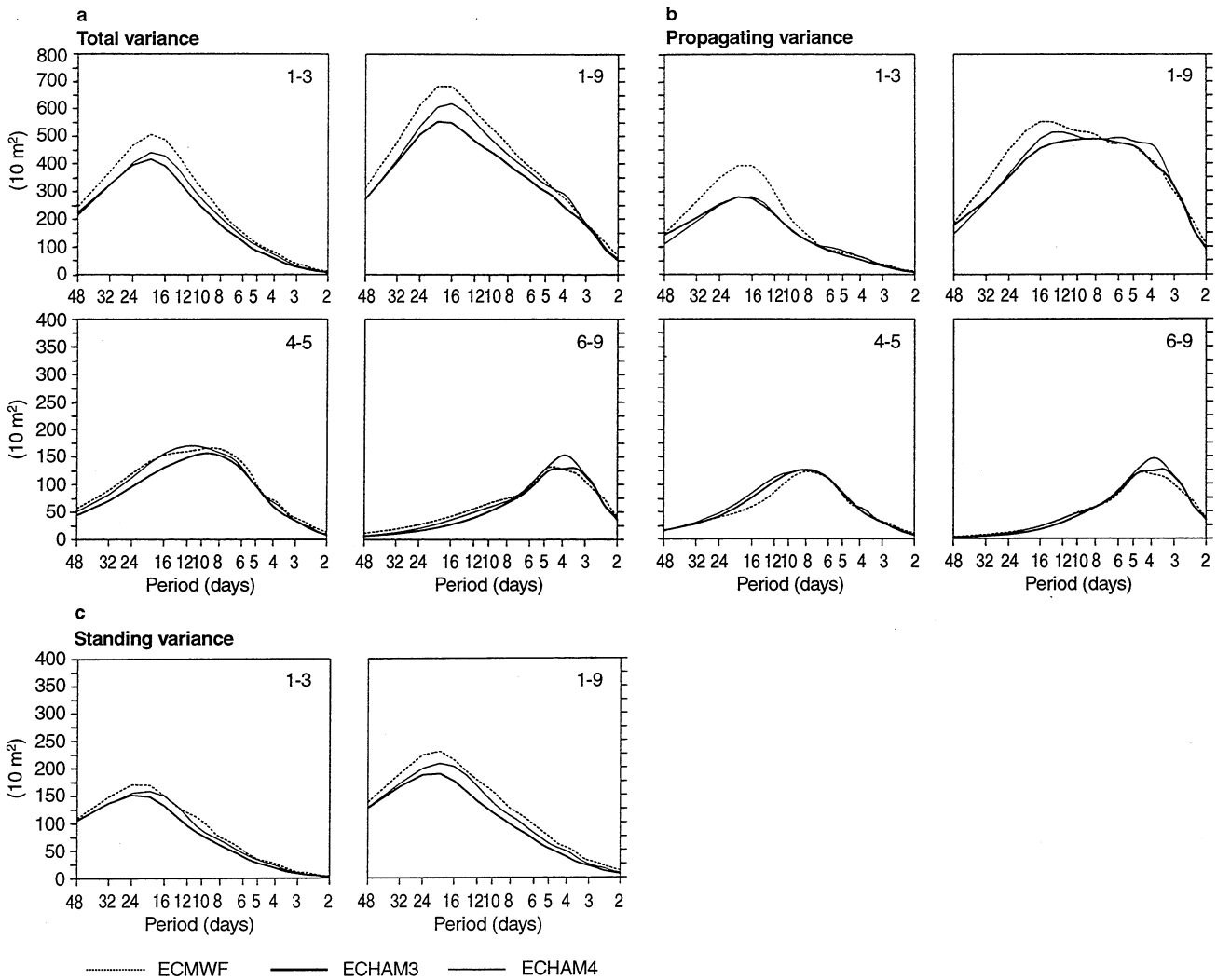

Fig. 5a–c Variance spectra of the geopotential height at 500 hPa in boreal winter between 40°–70 °N obtained from the ECMWF re-analyses and the simulations with ECHAM3 and ECHAM4, respectively, for three different planetary wave regimes: ultra-long (1–3), long (4–5), short (6–9) and all planetary scale waves (1–9). The spectral estimates are multiplied by frequency

(Fig. 4), however, these three spectral peaks are more apparent. Only the regime including the intermediate time scales between 6 and 10 days is somewhat suppressed. But similar to the simulations with ECHAM3 and in contrast to the re-analyses, these distinct regimes do not appear as clearly in the propagating variance spectrum, where merely the peak in the high-frequency part of the spectrum can be clearly identified.

In order to compare the results obtained from the three data sets directly, we present figures including the variance spectra for all data sets in the following. We distinguish between the three different wave regimes identified earlier. We classify ultra-long (zonal wave numbers 1–3), long (wave numbers 4–5) and short planetary wave (wave numbers 6–9) regimes. In addition the contributions of all planetary scale waves (wave numbers 1–9) are given. In these representations the spectral densities were multiplied by the frequency. In addition we present values of the variance computed from the various spectra, i.e., the total, propagating and standing variance spectra distinguishing between the wave regimes mentioned. According to a two-sided t-test the differences between the three different data sets, which are discussed in the following, are significant at a level of 95% or even 99%.

As seen in Figs. 5a and 7a, both the ECHAM3 and the ECHAM4 models generally underestimate the intraseasonal variability in the northern midlatitudes in boreal winter, in particular the variability caused by the ultra-long waves (1–3), which give major contributions for the long time scales. The contributions of the long (4–5) and short waves (6–9), on the other hand, are considerably better reproduced by the ECHAM model. In the simulations with ECHAM4 the intraseasonal variability is generally, that is on all spatial and temporal scales, stronger than in the simulations with ECHAM3. The standing variance spectra (Fig. 5c) give the same kind of relationships between the three data

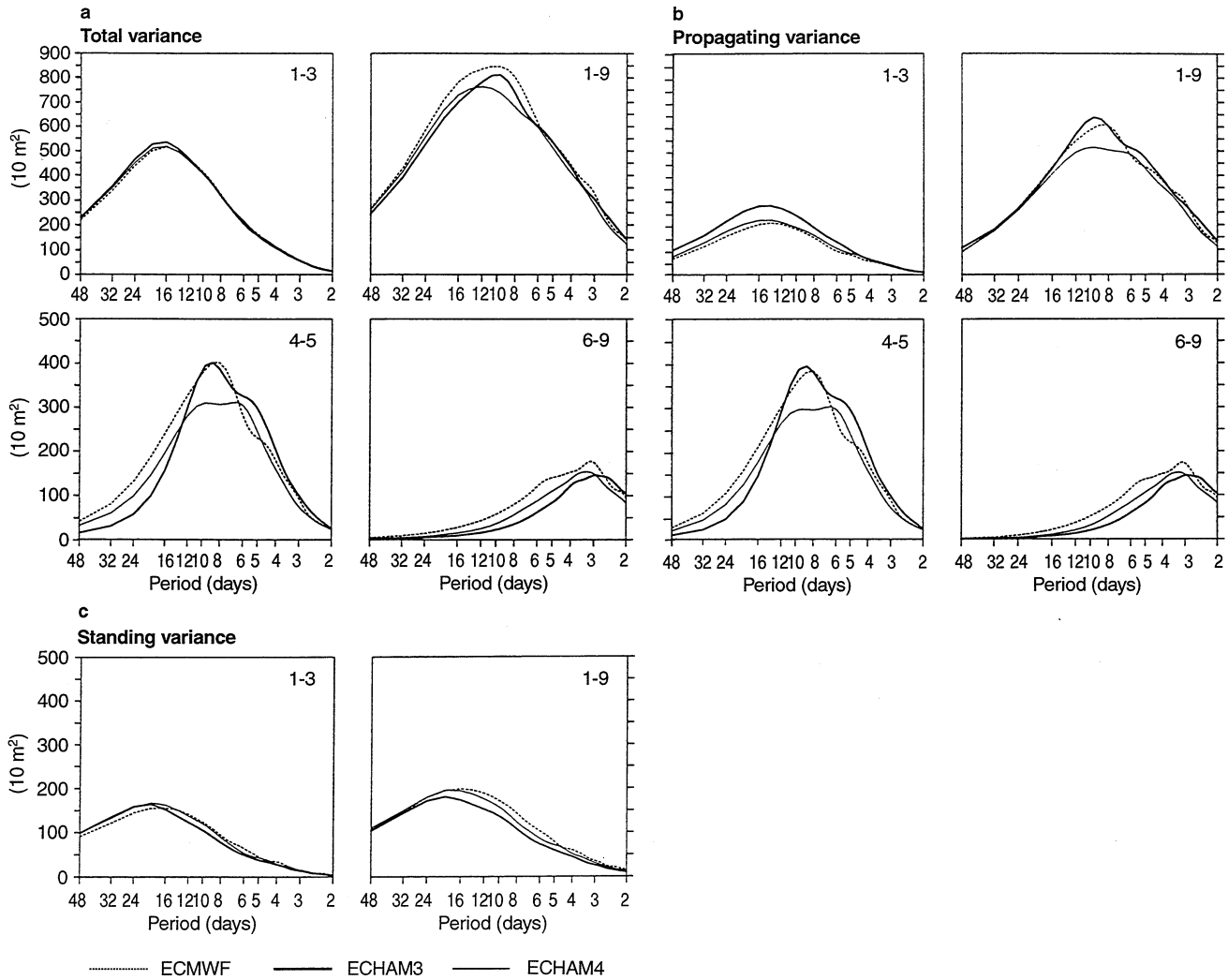

Fig. 6a–c As Fig. 5, but in austral winter between 40°–70 °S

sets as the total spectra, whereas the propagating variance spectra display a more complicated behaviour (Fig. 5b). In the low-frequency part of the spectrum the activity of the ultra-long propagating waves (1–3) is considerably underestimated in both sets of simulations. The contributions of the long planetary waves (4–5) on time scales longer than 6 days and of the short planetary waves (6–9) on time scales shorter than 6 days, on the other hand, are overestimated by the models.

4.2.2 Southern Hemisphere

As in the Northern Hemisphere the variance spectra in the Southern Hemisphere obtained from the two sets of simulations with the ECHAM model in austral winter (Fig. 3 and Fig. 4) have the same general structure as seen in the re-analyses (Fig. 2). The main differences to be noted are a reduction in the spectral peak at wave numbers 3 and 4 in the simulations with ECHAM4 (Fig. 4) and an increase in the peak at wave numbers 5 and 6 in the simulations with ECHAM3 (Fig. 3). These discrepancies are mainly accounted for by the different characteristics of the propagating waves on intermediate and short time scales, as can be seen in the propagating wave spectra. The standing variance spectra obtained from the two sets of simulations, on the other hand, are in good agreement with the spectrum derived from the re-analyses.

These differences can be seen better from the direct comparison of the total variance spectra obtained from the different data sets (Figs. 6a and 7). In the simulations with ECHAM4 the variance caused by the waves at zonal wave numbers 4 and 5 is considerably reduced for periods between 6 and 12 days, whereas on shorter time scales of 3 to 6 days the contributions of these waves to the intraseasonal variability is enhanced in the simulations with ECHAM3. The contributions of the short waves (6–9) are generally reduced in both models, somewhat more in ECHAM3 than in ECHAM4. The

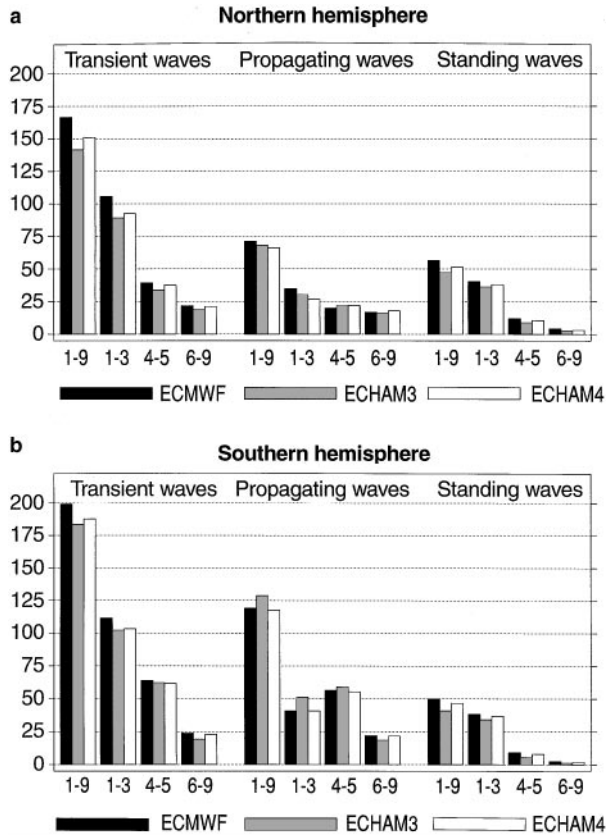

Fig. 7a, b Values of the variance computed from different spectra, that are the total, propagating and standing variance spectra of the geopotential height at 500 hPa distinguishing between different data sets and different planetary wave regimes (see text). The values represent area averages over the zone between 40° and 70 °N in **a** boreal winter and **b** over the zone between 40° and 70 °S in austral winter. Units are 100 m^2

differences described above can also be found in the propagating variance spectra (Fig. 6b). These spectra also indicate an overestimation of the contributions of the ultra-long waves (1–3) to the variance in ECHAM3. The standing variance spectra (Fig. 6c), on the other hand, show a considerable underestimation of the variance in ECHAM3, but only a slight underestimation of the variance in the recent version of the ECHAM model. A careful inspection of Fig. 7b reveals the general improvement of the simulation of the spectral distribution of the variance in the southern midlatitudes in ECHAM4 relative to the previous version of the model.

5 Signature of the ENSO phenomenon: ECMWF re-analyses

In the following we investigate the impact of the pronounced variations of the SSTs in the tropical Pacific associated with the ENSO phenomenon on the intraseasonal variability in the extratropics, in particular on the spectral distribution of the contributions of the transient fluctuations. For this purpose we compute composites depending on the phase of ENSO.

In the period of investigation between 1979 and 1993 we find three complete cycles of negative and subsequent positive SST-anomalies in the eastern part of the tropical Pacific basin, that is the Niño-3-region (e.g. Kousky et al. 1996). We classify the ENSO-events according to the occurrence of pronounced SST-anomalies in this region. In the boreal winter season we consider the winters in 1982/83, 1986/87, 1991/92 and 1992/93 (only for the ECMWF re-analyses and the simulations with ECHAM4) to be affected by an El Niño or warm ENSO-event, and in 1980/81, 1984/85 and 1988/89 by a La Niña or cold ENSO-event. The remaining seven boreal winters have been assigned to the control cases. The characteristics of these ENSO-events except for the El Niño event in 1992/93 are described in further detail in May and Bengtsson (1998).

5.1 Analysis of variance

Figure 8 and Table 1 show the contributions of the transient cell and of the stationary and transient eddies

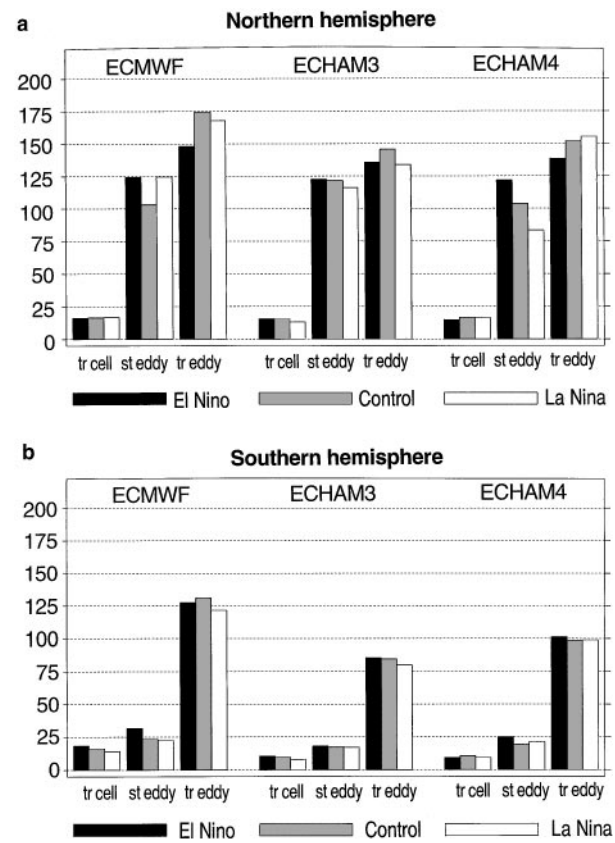

Fig. 8a, b Contributions of the transient cell and the stationary and transient eddies to the variance of the geopotential height at 500 hpa distinguishing between El Niño and La Niña events and control cases for different data sets. The values represent area averages over the zone between 40° and 70° **a** northern and **b** southern latitude, respectively, in boreal winter. Units are 100 m^2

Table 1a Contributions of the transient cell and the stationary and transient eddies to the variance of the geopotential height at 500 hPa distinguishing between El Niño and La Niña events and control cases for different data sets. The values represent area averages over the zone between 40° and 70° northern latitude in boreal winter (see Fig. 8a). Units are 100 m^2. For the simulations with the ECHAM model the significance of the difference between El Niño events and the control cases, the difference between La Niña events and the control cases (to the right of the respective numbers) and of the difference between El Niño and La Niña events (to the left of the respective numbers) is indicated by the asterisks. Four asterisks denote a significance level of more than 99%, 3 a level of more than 95%, 2 a level of more than 90%, and 1 a level of more than 75%

		NH (40–70 °N)		
	Composite	Transient cell	Stationary eddies	Transient eddies
ECMWF	El Niño	16.2	124.4	148.1
	La Niña	16.7	124.6	167.7
	Control	16.5	103.2	174.5
ECHAM3	El Niño	**15.5	122.7	135.8***
	La Niña	13.1***	116.1	133.9**
	Control	15.5	121.7	145.8
ECHAM4	El Niño	*14.7	****122.0**	***138.6***
	La Niña	16.3	83.4***	155.3
	Control	16.5	103.7	151.8

Table 1b As Table a but for the zone between 40° and 70 °S (see Fig. 8b)

		SH (40–70 °N)		
	Compoite	Transient cell	Stationary eddies	Transient eddies
ECMWF	El Niño	18.3	31.7	127.6
	La Niña	14.1	22.3	121.6
	Control	15.9	23.3	131.1
ECHAM3	El Niño	****10.6	18.1	***85.3
	La Niña	7.8****	17.1	79.8***
	Control	9.8	17.4	84.4
ECHAM4	El Niño	9.3*	*25.0***	101.4
	La Niña	9.3**	21.2	99.0
	Control	10.6	19.3	98.3

to the variance of the geopotential height field at 500 hPa, distinguishing between El Niño and La Niña events and the control cases in boreal winter. For the simulations with the ECHAM model (see Sect. 6.1), in addition to the estimates of the variance, the significance of the difference between El Niño events and the control cases, the difference between La Niña events and the control cases and the difference between El Niño and La Niña events is indicated in the Table 1. A very high significance of 99% is denoted by four symbols, a modest significance of 75% by one symbol, etc.. Since the values derived from the model data are based on an ensemble of five and two simulations, respectively, we are able to include 15 (8) El Niño events, 15 (6) La Niña events and 35 (14) control cases in the statistical test for ECHAM3 (ECHAM4), so that the statistical tests are more robust.

According to the ECMWF re-analyses the variance associated with the transient cell in the Northern Hemisphere extratropics is stronger during La Niña than during El Niño events (Fig. 8a and Table 1a). This is also the case for the contribution of the transient eddies to the variance, whereas the activity of the stationary eddies is only slightly greater during warm ENSO events than during cold ones. As a result, the overall variance is stronger during La Niña (30 900 m^2) than during El Niño events (28 870 m^2). These findings are to some extent in very good agreement with results obtained by Fraedrich and Müller (1993), who studied the impact of the ENSO phenomenon on the variability of the geopotential height field along 50 °N. They also observed an enhancement of the variance associated with the transient cell and with the transient eddies during La Niña events, but found a reduction of the variance due to the stationary eddies during cold ENSO-events as well. Their findings indicated that the activity of the transient disturbances is enhanced (reduced) at the expense (benefit) of the stationary waves during La Niña (El Niño) events. When comparing our results with those of Fraedrich and Müller (1993) one must keep two things in mind. First of all the sampling problem is much less severe in their study, since they have been investigating data from a much longer period. On the other hand they have been looking at one

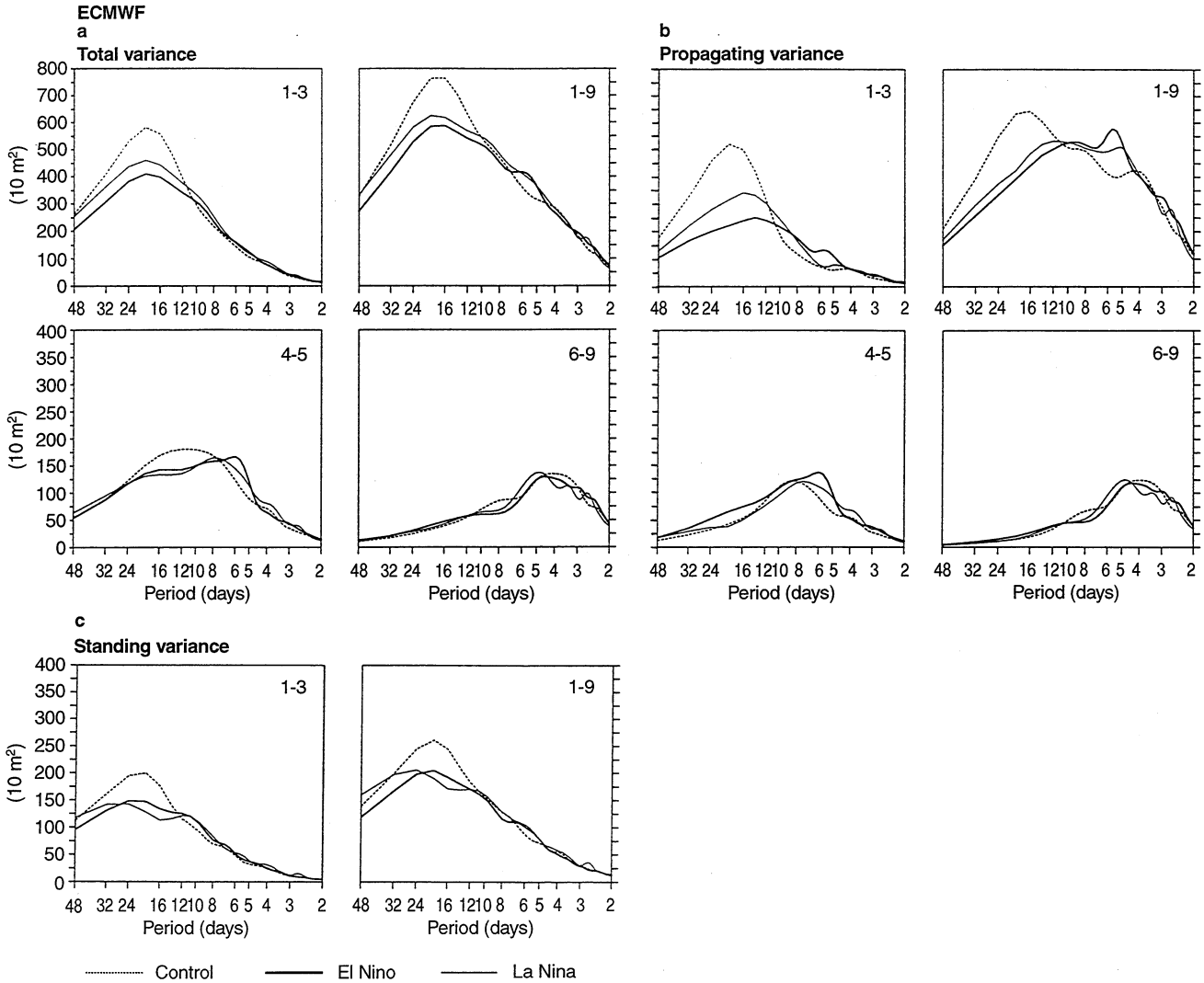

Fig. 9a–c Variance spectra of the geopotential height at 500 hPa in boreal winter between 40°–70 °N obtained from the ECMWF re-analyses for El Niño and La Niña events and the control cases, respectively, distinguishing between three different planetary wave regimes: ultra-long (1–3), long (4–5), short (6–9) and all planetary scale waves (1–9). The spectral estimates are multiplied by frequency

particular parallel of latitude only, so that their results may also reflect a meridional shift of the same kind of circulation rather than a change in the circulation pattern associated with an ENSO-event.

In the Southern Hemisphere, however, all the different contributions to the variance are stronger during El Niño than during La Niña events (Fig. 8b and Table 1b), leading to an overall estimate of the variance of 17 760 m^2 versus 15 800 m^2 during the warm and cold ENSO-events, respectively. It is interesting to note that the contribution of the transient eddies is greater for the control cases than during the different ENSO-events. This is also the case in the Northern Hemisphere (Fig. 8a).

5.2 Wave number-frequency spectra

In the following we investigate how the spectral distribution of the contribution of transient fluctuations to the intraseasonal variability in the extratropics is effected by the ENSO phenomenon. Analogous to Sects. 3.2 and 4.2 we present wave number-frequency spectra of the geopotential height at 500 hPa distinguishing between El Niño and La Niña events and the control cases.

Both the total and the propagating variance spectra in the northern midlatitudes in boreal winter obtained from the ECMWF re-analyses (Figs. 9a, 9b) are characterized by a considerable reduction of the low-frequency part of the intraseasonal variability during the warm as well as during cold ENSO-events, which is mainly accounted for by the reduced activity of the ultra-long planetary waves (1–3) during ENSO-events. Moreover, the low-frequency variability is stronger during La Niña than during El Niño events. Considering the long synoptic waves (4–5), the re-analyses indicate a shift in the variance to shorter temporal scales during the different ENSO-events. On time scales

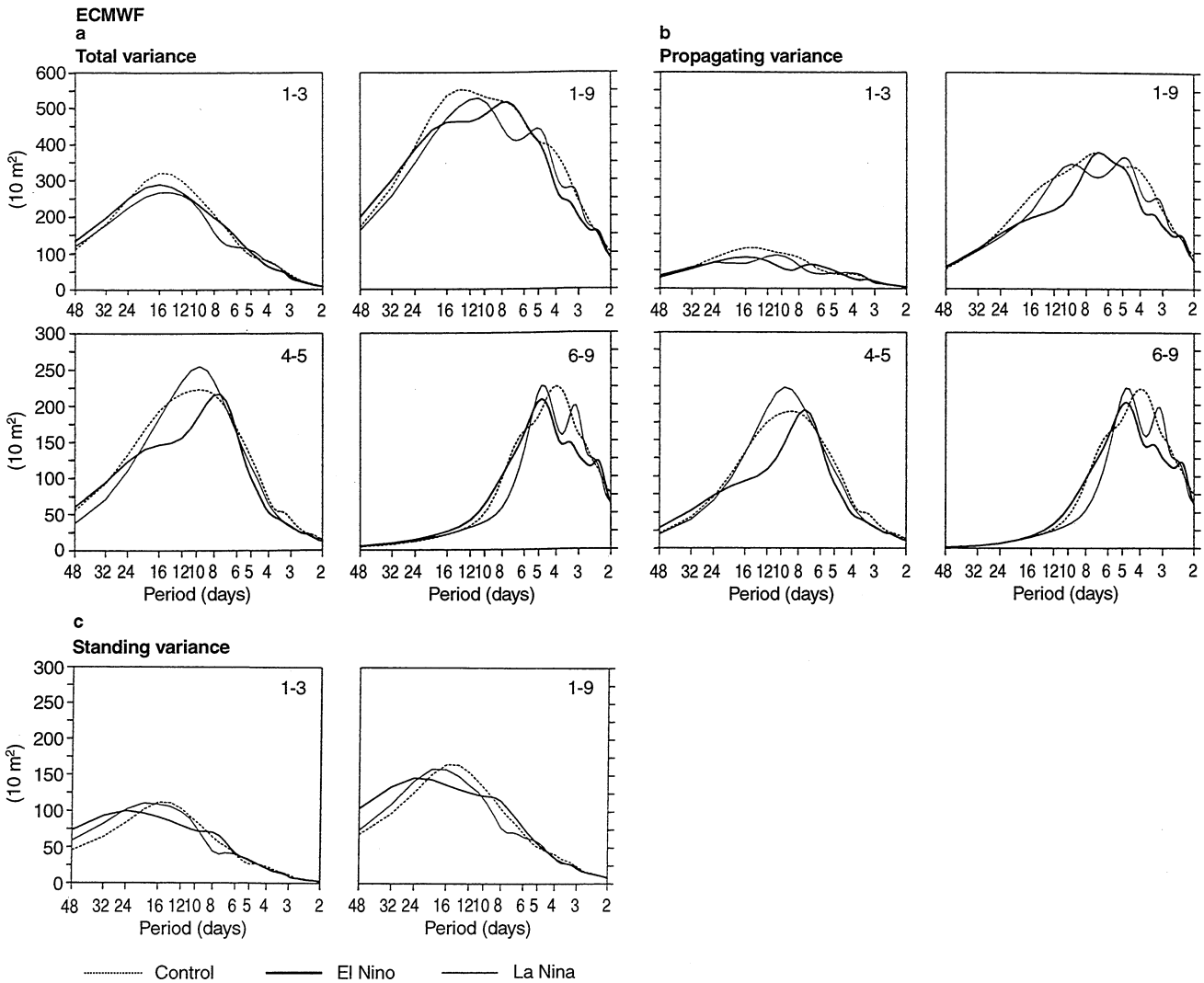

Fig. 10a–c As Fig. 9, but for 40°–70 °S

between 8 and 24 days the variance is considerably greater for the control cases, while on time scales between 5 and 8 days it is greater during El Niño as well as during La Niña events with values during warm ENSO-events exceeding those during cold ones.

The standing variance spectra (Fig. 9c) show a somewhat different behaviour. As for the ultra-long propagating waves, the contributions of the ultra-long standing waves to the intraseasonal variability are considerably reduced during both El Niño and La Niña events. The main difference between El Niño and La Niña events is a shift in the major contributions of these waves to longer temporal scales during cold ENSO-events compared to warm ones. This is in agreement with the result obtained by Hansen et al. (1989), according to which the contribution of the standing waves to the intraseasonal variability on these long time scales is substantially stronger during the cold than during warm ENSO-events. The propagating variance spectrum, however, does not exhibit the enhanced activity of zonal wave 7 for a period of about 5 days during an "average" El Niño as found by Hansen et al. (1989) and Fraedrich and Müller (1993). One should however keep in mind that certain characteristics typical of an average El Niño or La Niña event may also occur during episodes which are not characterized by the respective SST-anomalies in the tropical Pacific (Hansen et al. 1989).

In the Southern Hemisphere the propagating variance spectra derived from the ECMWF re-analyses (Fig. 10b) show a reduction of the contribution of the ultra-long waves (1–3) during both El Niño and La Niña events. Also the activity of the synoptic waves (4–5 and 6–9) is reduced during warm ENSO-events, whereas the contributions of these waves are enhanced during the cold events. In this case the spectrum reveals two peaks, one for zonal wave 6 for a period of 5 days and one for zonal wave 7 for a period of 3 days. The standing variance spectra (Fig. 10c) are characterized by an enhancement of the variance for very long time scales during both warm and cold ENSO-events. The

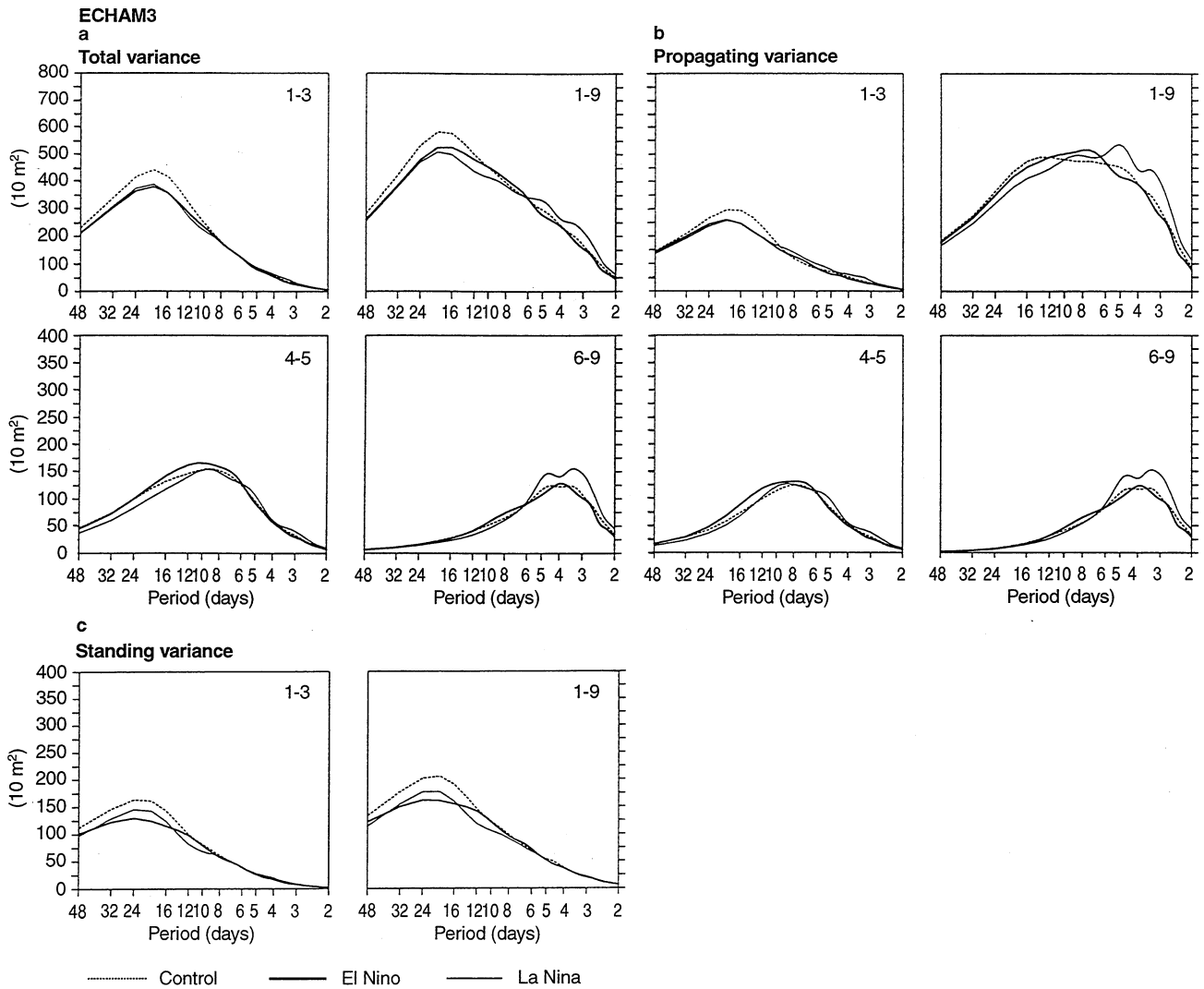

Fig. 11a–c As Fig. 9, but for the simulations with ECHAM3

spectra also show a shift in the major contributions of these waves to longer temporal scales during La Niña events compared to El Niño events, in contrast to the Northern Hemisphere, where we find the opposite behaviour (Fig. 9c). The total variance in the low-frequency part of the spectrum is reduced during both warm and cold ENSO-events, and the variance on these time scales is stronger during La Niña than during El Niño events (Fig. 10a).

6 Signature of the ENSO phenomenon: ECHAM model

6.1 Analysis of variance

The simulations with ECHAM4 show the same impact of the ENSO phenomenon on the characteristics of the variability in the Northern Hemisphere extratropics as the ECMWF re-analyses, whereas the simulations with ECHAM3 only agree in part with the re-analyses (Fig. 8a and Table 1a). The features, which all three data sets have in common and therefore can be considered as robust, are mainly associated with El Niño events, namely an enhancement of the activity of the stationary waves compared to the control cases at the expense of the transient waves. The impact of La Niña events, on the other hand, varies between the different data sets and, hence, is more uncertain. In the Southern Hemisphere (Fig. 8b and Table 1b), however, the impact of the ENSO phenomenon on the variability in the extratropics, that is an enhancement of all the different contributions to the variance during El Niño compared to La Niña events, can be found in all three data sets and, hence, is a robust result of this study.

6.2 Wave number-frequency spectra

In agreement with the ECMWF re-analyses (Fig. 9) both models simulate a reduction of the low-frequency

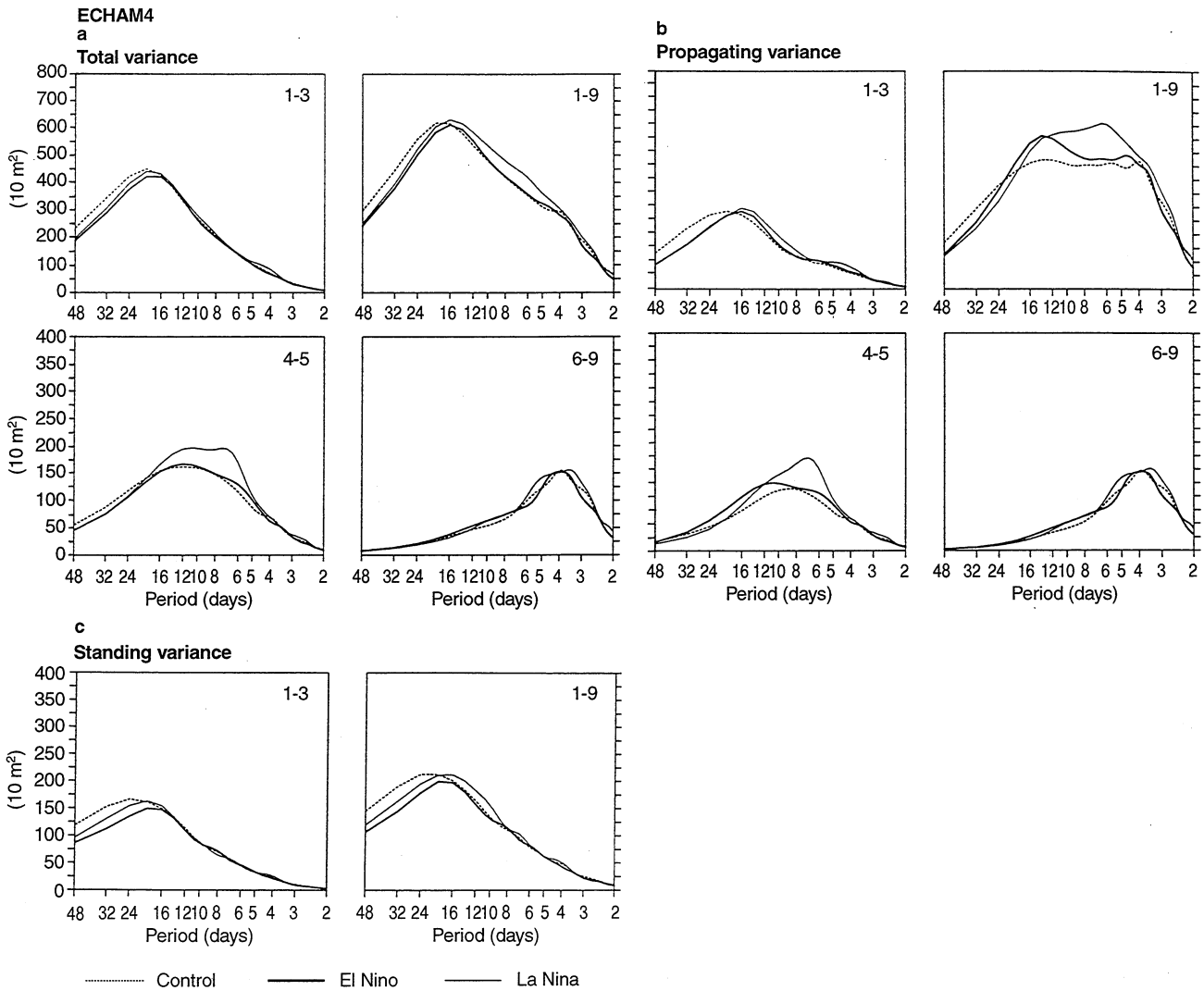

Fig. 12a–c As Fig. 9, but for the simulations with ECHAM4

part of the intraseasonal variability in the Northern Hemisphere extratropics during both warm and cold ENSO-events (Figs. 11 and 12). This is due to a reduction of the activity of the propagating as well as of the standing ultra-long waves (1–3). In the Southern Hemisphere the variance spectra obtained from two sets of simulations (Figs. 13 and 14) show a greater activity of ultra-long waves (1–3) during La Niña then during El Niño events in agreement with the re-analyses (Fig. 10). Other effects of the ENSO phenomenon on the spectral distribution indicated in the re-analyses, however, are not found in the two sets of simulations, indicating that they may not be robust.

7 Summary and concluding remarks

The comparison between the results obtained from two sets of simulations with the ECHAM3 and ECHAM4 atmospheric GCM with the results obtained from the ECMWF re-analyses has revealed that both models realistically reproduce many aspects of the intraseasonal variability in the extratropics. Both models show the partition of the variability into the contributions of the transient cell and of the stationary and transient eddies, and also the spectral distribution of the contributions of the transient waves in very good agreement with the re-analyses. In addition, they reveal the same seasonal variations and interhemispheric differences of the different contributions to the intraseasonal variability as in the re-analyses. In the recent version of the ECHAM model (ECHAM4) some of the model's shortcomings in simulating the intraseasonal variability realistically, in particular those in the Southern Hemisphere, are noticeably reduced compared to the previous version (ECHAM3). Yet some aspects are more realistically captured by ECHAM3. Apparently the reduction of the errors in the simulation of the temperature and wind fields within the extratropical

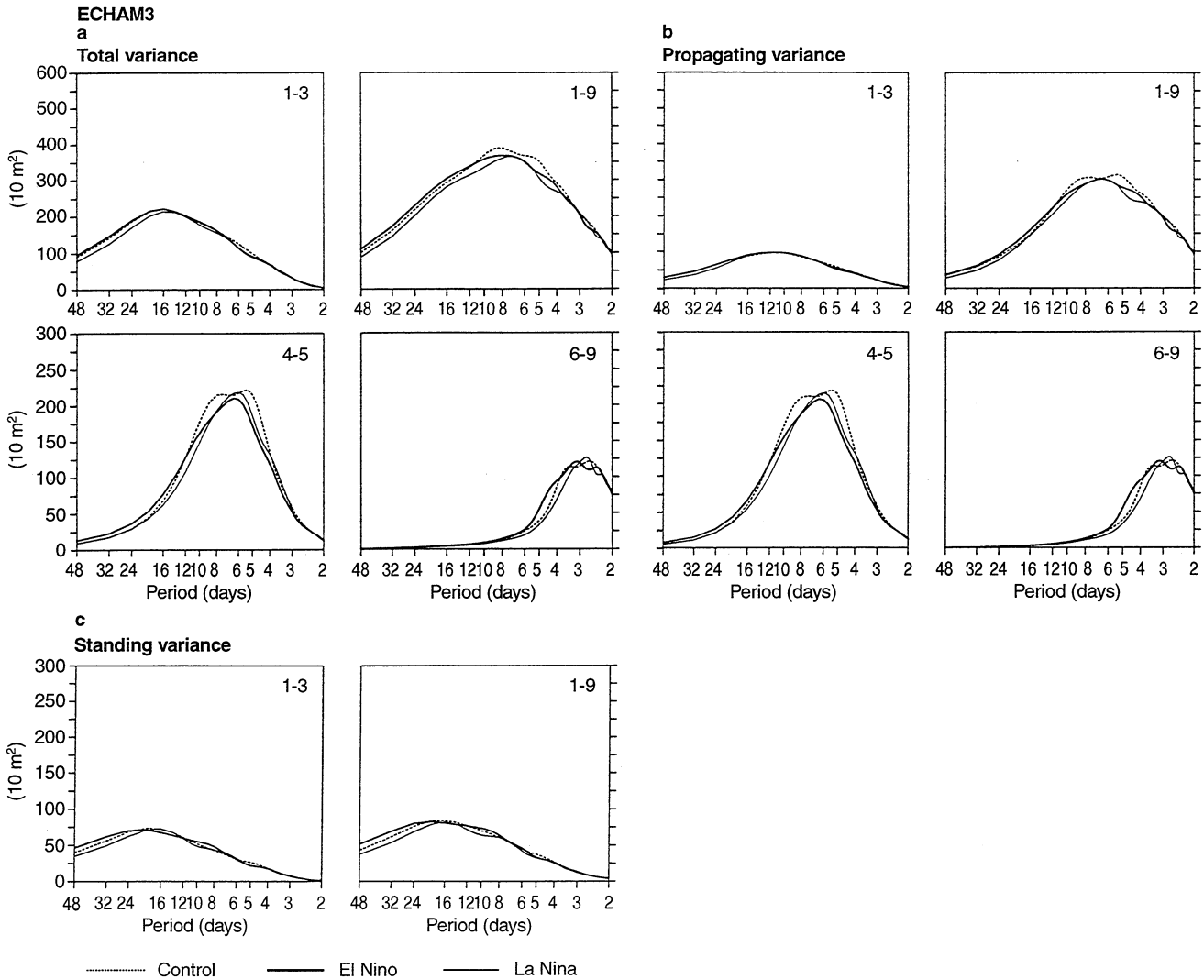

Fig. 13a–c As Fig. 10, but for the simulations with ECHAM3

troposphere in ECHAM4 (Roeckner et al. 1996) is accompanied by an improvement of the simulation of many aspects of the intraseasonal variability in the midlatitudes.

The most severe deficiency of the ECHAM model, i.e., the underestimation of the low-frequency part of the intraseasonal variability within the Northern Hemisphere midlatitudes due to an underestimation of the contributions of ultra-long transient waves, is certainly reduced in ECHAM4, but the variability on these scales is still too weak. The most obvious candidate leading to this improvement is the parametrization of the horizontal diffusion, where the order of the scheme has been increased. By these means the damping is confined to higher wave numbers, and non-linear interactions between disturbances on different scales cover a broader spectrum. A parametrization, which has not been changed, is the parametrization of the gravity wave drag (Miller et al. 1989). Hence the effects of the orography on the atmospheric circulation and therewith also on the low-frequency intraseasonal variability, which are essential in the Northern Hemisphere, are virtually the same in both versions of the model.

Both the ECMWF re-analyses and the two sets of simulations with the ECHAM model have shown a distinct impact of the ENSO phenomenon on the characteristics of the intraseasonal variability in the extratropics in boreal winter. In the Northern Hemisphere all three data sets reveal an enhancement of the activity of the stationary waves relative to the control cases at the expense of the transient waves. In the Southern Hemisphere, on the other hand, all the different contributions to the variance on intraseasonal time scales (transient cell, stationary and transient eddies) are stronger during El Niño than during La Niña events. These changes in the activity of the transient waves during warm and cold ENSO-events mainly reflect changes in the low-frequency part of the spectrum associated with the activity of ultra-long planetary waves.

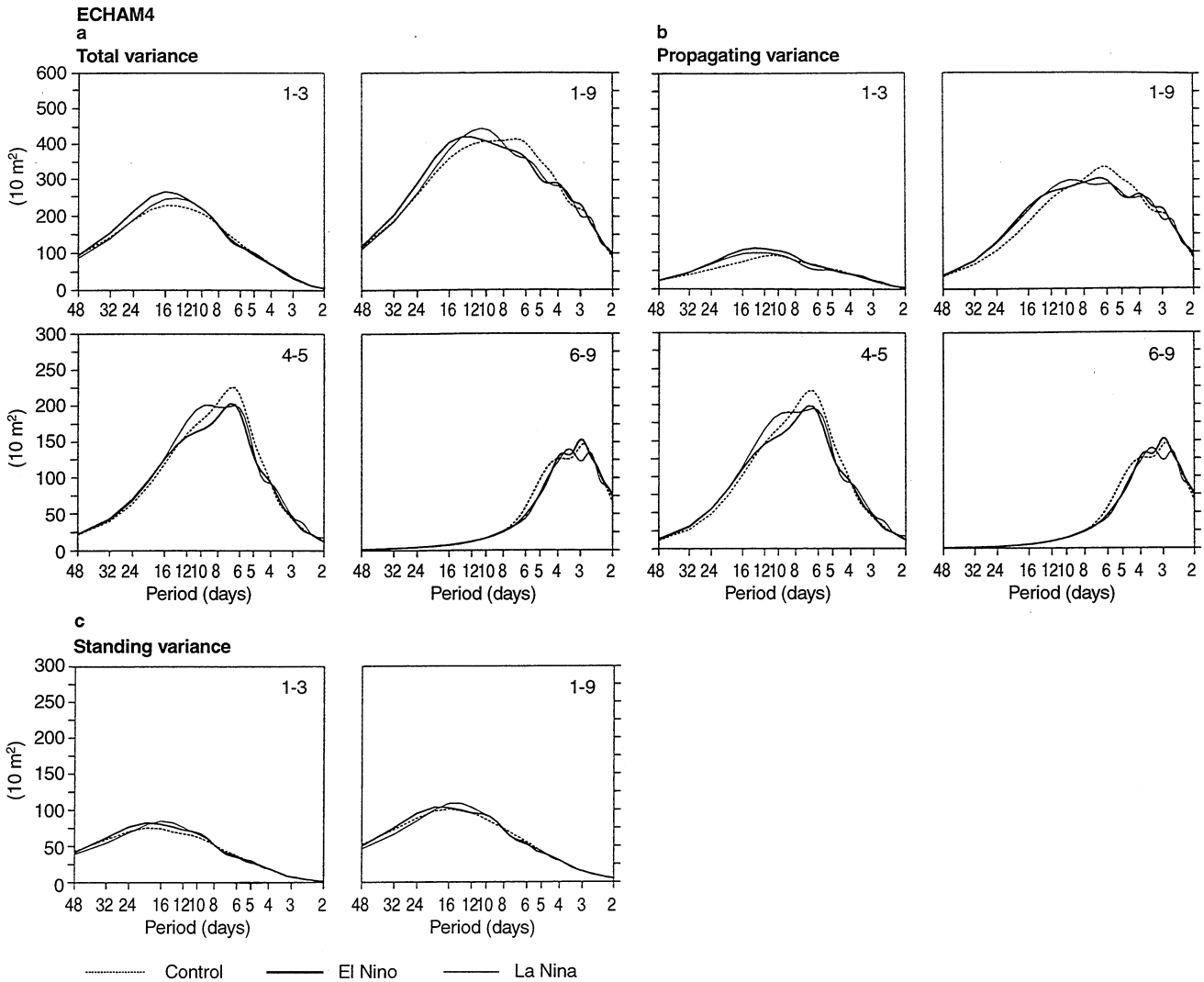

Fig. 14a–c As Fig. 10, but for the simulations with ECHAM4

An interesting and somewhat surprising result of our study has been that the low-frequency intraseasonal variability in the extratropics is reduced during both El Niño and La Niña events compared to the control cases. In the Northern Hemisphere this feature is rather robust, since it has been found in the re-analyses and in the two sets of simulations with the ECHAM models, while in the Southern Hemisphere only the re-analyses reveal this feature. An explanation for this behaviour, which occurs in the Pacific/North American as well as the Atlantic/European region (May and Bengtsson 1996), is not obvious, since the intraseasonal variability on these long time scales is strongly affected by non-linear processes and, moreover, can be caused by a variety of different phenomena. To some extent, however, these changes in the low-frequency intraseasonal variability could be related to changes in the characteristics of the high-frequency variability, since transient disturbances on synoptic time scales play an important role in forcing and/or maintaining blocking anticyclones (e.g. Mullen 1987). May and Bengtsson (1996) have noted changes in the occurrence of large-scale persistent flow anomalies in the Northern Hemisphere extratropics associated with the ENSO-phenomenon, which they could relate to changes in the characteristics of the storm tracks. That would mean that the forcing of the low-frequency fluctuations by the synoptic disturbances is reduced during ENSO-events, either due to a weakening of the of storm activity or due to a suppression of the forcing of large-scale flow anomalies leading to a stronger zonal orientation of the flow.

Acknowledgements I would like to thank the Max-Planck-Institute for Meteorology in Hamburg for providing the data from the simulations with the ECHAM model. My thanks go also to the two anonymous reviewers for their critical remarks, which helped to improve the manuscript.

Appendix A: analysis of variance

At a given latitude the geopotential height $\phi(x, t)$, which is given as a function of the longitude x and the time t, can be broken up into four terms: the temporal and zonal mean (temporal mean meridional circulation), the temporal fluctuations of the zonal mean (transient cell), the longitudinal fluctuations of the temporal mean (stationary eddies), and the combined temporal and longitudinal fluctuations (transient eddies). This is written as:

$$\phi(x, t) = [\phi]_{x,t} + ([\phi]_x)_t(t) + ([\phi]_t)_x(x) + (\phi)_{x,t}(x, t), \tag{A1}$$

where the longitudinal and temporal means are denoted by $[\ ]_x$ and $[\ ]_t$ and their respective departures by $(\ )_x$ and $(\ )_t$. Thus the total variance of the geopotential height field ($Var(\phi)$) due to longitudinal and temporal fluctuations, that is its longitudinal and temporal mean at this latitude, is given as follows:

$$\begin{aligned} Var(\phi) &= [(\phi(x, t) - [\phi]_{x,t})^2]_{x,t} \\ &= \underset{(I)}{[([\phi]_x)_t^2]_{x,t}} + \underset{(II)}{[([\phi]_t)_x^2]_{x,t}} + \underset{(III)}{[(\phi)_{x,t}^2]_{x,t}}. \end{aligned} \tag{A2}$$

According to this we can distinguish between the contributions of the transient cell (I) and of the stationary (II) and transient eddies (III) to the total variance of the geopotential height field.

We compute these terms for individual seasons, which are defined as segments of 90 days for the simulations and of varying length between 90 and 92 days for the analyses starting at March 1, June 1, September 1 and December 1, respectively. Furthermore, we transform the transient eddies into the wave number-frequency domain, so that we can separate the contributions of the transient fluctuations by their spatial and temporal scales (see Appendix B).

Appendix B: Wave number-frequency analysis

In order to distinguish the contributions of the transient eddies on different spatial and temporal scales to the atmospheric intraseasonal variability we perform a wavenumber-frequency analysis of the contributions of the transient eddies to the variance of the geopotential height. We estimate one-sided frequency spectra (Pratt 1976), which differ essentially from the two-sided frequency spectra as defined in Hayashi (1971) in the way the role of standing and propagating fluctuations is defined. For a detailed discussion of this problem we refer to Pratt (1976).

According to the method proposed by Hayashi (1971) the two-sided frequency spectrum (E) defines for a given zonal wave number k and frequency ω the components of the eastwardly ($+\omega$) and westwardly ($-\omega$) propagating waves in a frequency band centred at a frequency ω as

$$E(k, \pm\omega) = \tfrac{1}{4}[P_\omega(C_k) + P_\omega(S_k)] \pm \tfrac{1}{2} Q_\omega(C_k, S_k) \tag{A3}$$

where P_ω is the power and Q_ω the quadrature spectrum of the time series of the cosine (C_k) and sine-coefficients (S_k) of the Fourier harmonics along a parallel of latitude. Using the cospectrum K_ω we derive the variance due to standing (ST) and due to zonally propagating fluctuations (PR) as follows:

$$ST(k, \omega) = \sqrt{K_\omega^2(C_k, S_k) + \tfrac{1}{4}[P_\omega(C_k) - P_\omega(S_k)]^2}, \tag{A4}$$

and

$$PR(k, \pm\omega) = E(k, \pm\omega) - \tfrac{1}{2} ST(k, \omega). \tag{A5}$$

These different spectra describe the connection between the time series of cosine- and sine-coefficients in the frequency domain. The power spectra, for instance, give the correlation within each of these series, the autocorrelation. The quadrature and cospectrum, on the other hand, represent the correlation between these two time series, the crosscorrelation. The crosscorrelation can be separated into two components giving the in-phase and the out-of-phase correlation between the two time series. A thorough description of the various spectra and of their connection is, for instance, given in Priestley (1981).

According to the method suggested by Pratt (1976) the total variance spectrum (T) is defined as the sum of the eastwardly and westwardly propagating contributions to the frequency spectrum given as in (A3), as

$$T(k, \omega) = \tfrac{1}{2}[P_\omega(C_k) + P_\omega(S_k)]. \tag{A6}$$

This spectrum represents the overall variance due to transient fluctuations. The propagating variance spectrum (PR), on the other hand, is defined as the difference between the eastwardly and the westwardly propagating waves defined as in (A5), as:

$$PR(k, \omega) = |Q_\omega(C_k, S_k)|. \tag{A7}$$

Therefore this spectrum gives the lower limit of the variance due to the propagating waves, whereas the separation into the eastwardly and westwardly propagating components according to (A5) sets the upper limit. The direction of the propagation along a parallel of latitude is given by the sign of Q_ω. Moreover, the sign indicates, whether for a given zonal wavenumber the eastwardly ($+$) or the westwardly propagating ($-$) component of the propagating wave dominates. If these two components are coherent, the two waves, which propagate with the same phase speed into opposite directions, interfere in such a way that they set up a standing wave. The contribution of the standing waves to the intraseasonal variance is given by the standing variance spectrum, which is also in Pratt (1976) defined as in (A4). It describes the temporal variability of the amplitudes of the standing waves.

The frequency spectra are estimated for the boreal and austral winter seasons. These are defined as segments of 96 days starting at December 1 and June 1, respectively. Before the computation of the spectra, the mean annual cycle and the residual mean are removed from the data. In addition, a potential linear trend is excluded. In order to obtain smooth spectral estimates, a Tukey-Hanning window with a time-lag of 20 days is applied (e.g. Priestley 1981). This window has a bandwidth of 1/15 cycles per day with an equivalent number of degrees of freedom of 13.

References

Bengtsson L, Arpe K, Roeckner E, Schulzweida U (1996) Climate predictability experiments with a general circulation model. Clim Dyn 12:261–278

Blackmon ML (1976) A climatological spectral study of the 500 mb geopotential height in the Northern Hemisphere. J Atmos Sci 33:1607–1623

Blackmon ML, Mullen SL, Bates GT (1986) The climatology of blocking in a perpetual January simulation of a spectral general circulation model. J Atmos Sci 43:1379–1405

Brinkop S, Roeckner E (1995) Sensitivity of a general circulation model to parametrizations of cloud-turbulence interactions in the atmospheric boundary layer. Tellus 47 A:197–220

Claussen M, Lohmann U, Roeckner E, Schulzweida U (1994) A global data set of land-surface parametrization. MPI-Report 135, 30 pp

Deland RJ (1972) On the spectral analysis of traveling waves. J Meteorol Soc Japan 50:125–128

DKRZ (1992) The ECHAM3 atmospheric general circulation model. Techn Rep 6, 184 pp

Essenwanger OM (1986) Elements of statistical analysis. In: Landsberg HE (Ed), World Survey of Climatology Vol. 1B, Elesvier Science Publishers Amsterdam, 424 pp

Fouquart Y, Bonnel B (1980) Computations of solar heating of the Earth's atmosphere: a new parametrization. Contrib Atmos Phys 53:35–62

Fraedrich K, Böttger H (1978) A wave number-frequency analysis of the 500 mb geopotential at 50 °N. J Atmos Sci 35: 745–750

Fraedrich K, Kietzig E (1983) Statistical analysis and wave number-frequency spectra of the 500 mb geopotential along 50 °S. J Atmos Sci 40: 1037–1045

Fraedrich K, Müller K (1993) Climatology of wave number-frequency spectra at 500 mb height along 50 °N during the El Niño/Southern Oscillation extremes. Meteorol Z 2: 80–84

Gates WL (1992) The atmospheric intercomparison project. Bull Am Meteorol Soc 73: 1962–1970

Gibson JK, Kållberg P, Uppala S, Hernandez A, Nomura A, Serrano E (1997) ERA description. ECMWF Re-analysis Project Report Series 1, 72 pp

Giorgetta M, Wild M (1995) The water vapor continuum and its representation in ECHAM4. MPI-Report 162, 38 pp

Hansen AR, Sutera A, Venne DE (1989) An examination of midlatitude power spectra: evidence for standing variance and the signature of El Niño. Tellus 41 A: 371–384

Hayashi Y (1971) A generalized method of resolving disturbances into progressive and retro- gressive waves by space Fourier and time spectral analysis. J Meteorol Soc Japan 49: 125–128

Hayashi Y (1982) Space-time spectral analysis and its applications to atmospheric waves. J Meteorol Soc Japan 60: 156–171

Hayashi Y, Golder DG (1977) Space-time spectral analysis of midlatitude disturbances appearing in a GFDL circulation model. J Atmos Sci 34: 237–262

Hayashi Y, Golder DG (1983) Transient planetary waves simulated by GFDL spectral general circulation models. Part I: effects of mountains. J Atmos Sci 40: 941–950

Hayashi Y, Golder DG (1993) Tropical 40–50- and 25–30-day oscillations appearing in realistic and idealized GFDL climate models and the ECMWF dataset. J Atmos Sci 50: 464–494

Hoerling MP, Blackmon ML, Ting M (1992) Simulating the atmospheric response in the 1985- 87 El Niño cycle. J Clim 5: 669–682

Kousky VE, Bell GD, Halpert MS, Higgins W (1996) Climate Diagnostics Bulletin 96/12, 78 pp

May W (1994) On the intra-seasonal variability within the extratropics in the ECHAM3 general circulation model. MPI-Report 147, 207 pp

May W, Bengtsson L (1996) On the impact of the El Niño/Southern Oscillation phenomenon on the atmospheric circulation in the Northern Hemisphere extratropics. MPI-Report 224, 61 pp

May W, Bengtsson L (1998) The signature of ENSO in the Northern Hemisphere midlatitude seasonal mean flow and intraseasonal variability. Meteorol Atmos Phys 69: 81–100

Mechoso RC, Hartmann DL (1982) An observational study of traveling planetary waves in the Southern Hemisphere. J Atmos Sci 39: 1921–1935

Miller MJ, Palmer TN, Swinbank R (1989) Parametrization and influence of sub-grid scale orography in general circulation and numerical weather prediction models. Meteorol Atmos Phys 40: 84–109

Morcrette J-J (1991) Radiation and cloud radiative processes in the European Centre for Medium Range Weather Forecasts forecasting system. J Geophys Res 96: 9121–9132

Mullen SL (1987) Transient eddy forcing of blocking flows. J Atmos Sci 44: 3–22

Nordeng TE (1994) Extended versions of the convective parameterization scheme at ECMWF and their impact on the mean climate and transient activity of the model in the tropics. ECMWF Research Department Techn Memo 206, 41 pp

Pratt RW (1976) The interpretation of space-time spectral quantities. J Atmos Sci 33: 1060–1066

Pratt RW (1979) A space-time spectral comparison of the NCAR and GFDL general circulation models of the atmosphere. J Atmos Sci 36: 1681–1691

Pratt RW, Wallace JM (1976) Zonal propagation characteristics of large-scale fluctuations in the mid-latitude troposphere. J Atmos Sci 33: 1184–1194

Priestley MB (1981) Spectral analysis and time series. Academic Press, London, 890 pp

Rex DF (1950a) Blocking action in the middle troposphere and its effect upon regional climate, I. An aerological study of blocking action. Tellus 3: 196–211

Rex DF (1950b) Blocking action in the middle troposphere and its effect upon regional climate, II. The climatology of blocking. Tellus 3: 275–301

Reynolds RW (1988) A real time global sea surface temperature analysis. J Clim 1: 75–86

Rockel B, Raschke E, Weyres B (1991) A parametrization of broad band radiative transfer properties of water, ice and mixed clouds. Contrib Atmos Phys 64: 1–12

Roeckner E, Arpe K, Bengtsson L, Brinkop S, Dümenil L, Esch M, Kirk E, Lunkeit F, Ponater M, Rockel B, Sausen R, Schlese U, Schubert S, Windelband M (1992) Simulation of the present-day climate with the ECHAM model: Impact of model physics and resolution. MPI-Report 93, 172 pp

Roeckner E, Arpe K, Bengtsson L, Christoph M, Claussen M, Dümenil L, Esch M, Giorgetta M, Schlese U, Schulzweida U (1996) The atmospheric general circulation model ECHAM-4: Model description and simulation of present-day climate. MPI-Report 218, 90 pp

Speth P, Madden RA (1983) Space-time spectral analysis of Northern Hemisphere geopotential heights. J Atmos Sci 40: 1086–1100

Tiedtke M (1989) A comprehensive mass flux scheme for cumulus parametrization in large-scale models. Mon Weather Rev 117: 1779–1800

Williamson DL, Rasch PJ (1994) Water vapor transport in the NCAR CCM2. Tellus 46 A: 34–51